Validation of Ray-Based Cross-Beam Energy Transfer Models

R. K. Follett,[1] A. Colaïtis,[2] D. Turnbull,[1] D. H. Froula,[1] and J. P. Palastro[1]

[1]Laboratory for Laser Energetics, University of Rochester
[2]Centre Lasers Intenses et Applications

This summary presents a series of comparisons between ray- and wave-based CBET calculations that highlight the essential physics that must be included in a ray-based CBET model. The comparison cases are designed to aid in the validation of ray-based CBET models by including precise input parameters and quantitative comparison metrics and/or wave-based field data.[1] The cases vary in complexity from simple 2-D two-beam interactions in a linear density gradient to 60 beams interacting in a 3-D spherical plasma profile. We have found that in all cases the most sophisticated algorithm (etalon integral field reconstruction[2] with a coherent caustic correction and caustic gain truncation[3]) performed at least as well as its more-simplistic counterparts without increasing the overall computational cost and should be the preferred algorithm for use in ray-based CBET codes. A particular emphasis is placed on energy conservation because ray-based CBET models typically do not conserve energy explicitly and require artificial correction. We show that the intrinsic lack of energy conservation inherent to ray-based algorithms significantly affects the accuracy and that artificially correcting energy-conservation errors can have a large impact on results.

In direct-drive inertial confinement fusion (ICF), a millimeter-scale spherical capsule is illuminated by symmetrically oriented laser beams.[4–6] The lasers ablate the outer layer of the capsule, which generates pressure to implode the fuel. In addition to depositing thermal energy in the ablator, the lasers can resonantly drive various laser–plasma instabilities (LPI's) that can degrade the quality of the implosion. One of the predominant LPI's that impacts ICF implosions is cross-beam energy transfer (CBET), where laser beams exchange energy through a ponderomotively driven ion-acoustic wave.[7,8] CBET reduces the overall laser absorption in direct-drive ICF because it tends to transfer energy from the incoming lasers to outgoing reflected/refracted light.

Many of the radiation-hydrodynamics codes used to design ICF implosions include CBET models, but implementation details vary significantly between codes and artificial multipliers are often required to reproduce experimental results.[2,3,8–16] One of the underlying reasons for the prevalence of artificial multipliers is that it is not clear what level of accuracy is even possible with ray-based codes because there are very few analytic results available for use as test cases. An excellent way to validate ray-based CBET models, however, is with wave-based calculations. Wave-based CBET models naturally include all of the physics that can only be approximately included in ray-based models. Due to the much higher computational cost, it is not currently possible to run 3-D wave-based CBET calculations at the scale of ICF experiments, but all of physics required for ray-based CBET models can be studied in subscale simulations.

The *LPSE* results are compared to ray-based results from two different codes. The first is a relatively simple test-oriented code that was developed in conjunction with *LPSE* for the specific purpose of making comparisons between ray-based CBET algorithms and *LPSE* results.[3] We also include results from the *IFRIIT*[2,13] laser deposition code implemented in 3-D *ASTER* (Ref. 17). *IFRIIT* provides an interesting comparison point because it implements some of the algorithms detailed in this summary for the electromagnetic-field calculation, while it differs significantly on other points—most notably on the use of inverse ray tracing versus forward ray tracing. Finally, it is an inline model, implying that contrary to the test-oriented ray-based code, it was formulated for speed while still being able to reproduce the *LPSE* results.

Figure 1 shows the laser absorption as a function of grid resolution for 2-D 16-beam simulations in an azimuthally symmetric plasma profile that is based on fits to a *LILAC* simulation of an OMEGA implosion. The various subfigures correspond to scaled versions of the original hydro profile ranging from 1/64th scale to full scale ($S = 1/64$ to $S = 1$). The various ray-based CBET models that were used are as follows: (1) "FL, no CGT" corresponds to field-limiter treatment of the caustic without caustic gain truncation (which leads to slow convergence); (2) "FL, no CC" corresponds to a field-limiter treatment of the caustic without using a coherent treatment of the fields in the caustic region (which leads to poor energy conservation); (3) "FL" corresponds to a field-limiter treatment with both CGT and a coherent caustic treatment; (4) "EI" corresponds to an etalon integral field reconstruction with both CGT and a coherent caustic treatment; (5) "*IFRIIT*" corresponds to results from the *IFRIIT* code that uses the same physical model as "EI" but with a different numerical implementation.
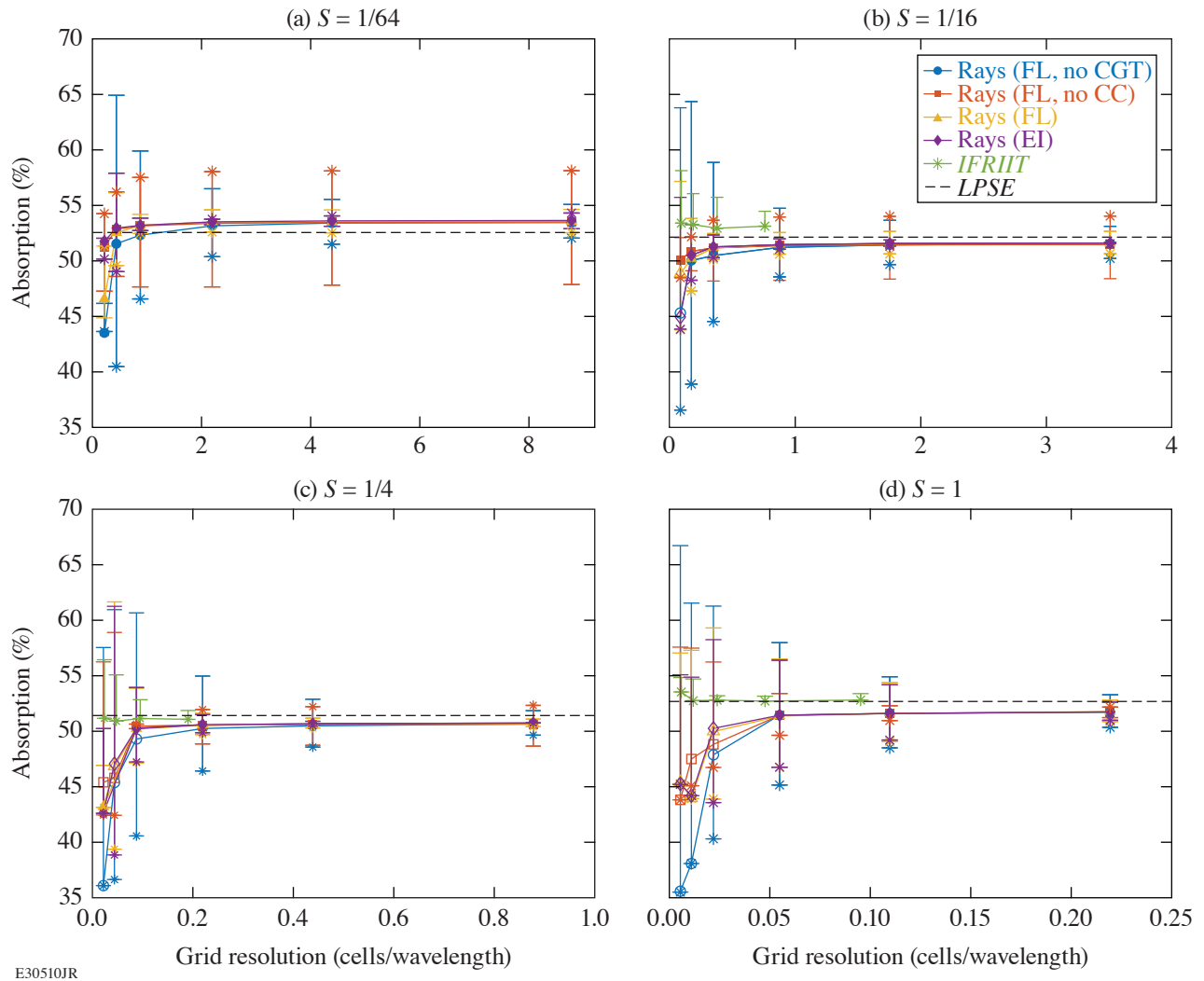

E30510JR

Figure 1

Laser absorption as a function of grid resolution for 16-beam 2-D simulations at (a) 1/64 scale, (b) 1/16 scale, (c) 1/4 scale, and (d) full scale. *LPSE* results are shown with horizontal black dashed lines. The stars represent the ray-based results without enforcing energy conservation, and the solid markers represent the energy-conserving results (open markers correspond to cases where energy conservation could not be achieved). The error bars show the size of the uncorrected energy-conservation error. The various ray-based approaches are FL without CGT (blue circles), FL without the coherent caustic correction (red squares), FL (yellow triangles), and EI (purple diamonds). The *IFRIIT* results are shown with green stars.

In all cases the converged ray-based results are in good agreement with the *LPSE* simulations ($\lesssim$1% difference in absorption). The ray-based results are plotted in a way that displays the absorption results and the energy-conservation properties on the same axes. Specifically, stars show the uncorrected absorption (energy conservation not enforced), and the solid markers show the absorption after enforcing energy conservation (open markers are used in cases where energy conservation could not be achieved). The range of the error bars corresponds to the range of absorption that could be achieved if all of the missing (extra) energy is added to (subtracted from) absorption or scattered (unabsorbed) light. Accordingly, any reasonable approach to enforcing energy conservation will result in an absorption within the error bar. Alternatively, a reasonable approach exists to enforcing energy conservation that would lead to any result between the error bars. An ideal algorithm would have the star on top of the solid marker (and vanishing error bounds), meaning that energy was conserved without any artificial correction. The results are plotted in this way because it is critically important to consider the impact of the somewhat arbitrary approach that is used to enforce energy-conservation ray-based CBET codes.

The "FL, no CC" model with $S = 1/64$ [Fig. 1(a)] provides a good example of why it is important to consider the uncorrected energy-conservation error. By simply comparing the converged solutions after correcting for energy conservation, the "FL, no CC" model gives the same result as the more-sophisticated models. However, the uncorrected energy-conservation error is greater than 10%, suggesting that the somewhat arbitrary choice of algorithm for enforcing energy conservation was a huge lever on the final result (the star being at the top of the error bar implies that extra energy was created). Conversely, the error bars using the EI method are much smaller ($\sim$1%), meaning that artificially enforcing energy conservation does not have a significant impact on those results. Note that the energy-conservation error (in the converged solution) tends to improve with increasing scale because a smaller fraction of the CBET is occurring in the caustic region. Achieving convergence at large scales can, however, be difficult because it becomes harder to resolve the caustics.

1. R. K. Follett, *LPSE* Data for Ray-Based CBET Test Cases (1.0.0) [Data set]. Zenodo (2022), Accessed 7 March 2023, http://dx.doi.org/10.5281/zenodo.6962934.
2. A. Colaïtis *et al.*, Phys. Plasmas **26**, 032301 (2019).
3. R. K. Follett *et al.*, Phys. Rev. E **98**, 043202 (2018).
4. J. Nuckolls *et al.*, Nature **239**, 139 (1972).
5. R. S. Craxton *et al.*, Phys. Plasmas **22**, 110501 (2015).
6. S. Atzeni and J. Meyer-ter-Vehn, *The Physics of Inertial Fusion: Beam Plasma Interaction, Hydrodynamics, Hot Dense Matter*, 1st ed., International Series of Monographs on Physics, Vol. 125 (Oxford University Press, Oxford, 2004).
7. C. J. Randall, J. R. Albritton, and J. J. Thomson, Phys. Fluids **24**, 1474 (1981).
8. P. Michel *et al.*, Phys. Plasmas **20**, 056308 (2013).
9. I. V. Igumenshchev *et al.*, Phys. Plasmas **19**, 056314 (2012).
10. A. Colaïtis *et al.*, Phys. Plasmas **23**, 032118 (2016).
11. J. A. Marozas *et al.*, Phys. Plasmas **25**, 056314 (2018).
12. A. Colaïtis *et al.*, Phys. Plasmas **25**, 033114 (2018).
13. A. Colaïtis *et al.*, J. Comput. Phys. **443**, 110537 (2021).
14. D. H. Edgell *et al.*, Phys. Plasmas **24**, 062706 (2017).
15. A. K. Davis *et al.*, Phys. Plasmas **23**, 056306 (2016).
16. D. J. Strozzi *et al.*, Phys. Rev. Lett. **118**, 025002 (2017).
17. I. V. Igumenshchev *et al.*, Phys. Plasmas **23**, 052702 (2016).